CHEMISTRY OF MATERIALS

pubs.acs.org/cm

Article

Open Access

This article is licensed under CC-BY 4.0

Structural Dispersity as a Determinant of Li-Ion Transport in Ethylene-Oxide-Based Graft Polymer Electrolytes

Anna Vigolo, Valeria Vanoli, Luca Laugeni, Carlos Pavón, Rossana Pasquino, Edmondo M. Benetti, Franca Castiglione,* and Francesca Lorandi*

Cite This: *Chem. Mater.* 2026, 38, 2063−2071

Read Online

ACCESS | Metrics & More | Article Recommendations | Supporting Information

ABSTRACT: Graft polymers with oligo(ethylene glycol) (OEG) side chains and poly(meth)acrylate backbones have been commonly studied as polymer electrolytes (PEs) owing to the ability of oligoether segments to coordinate Li^+ ions. However, when poly[oligo(ethylene glycol) methyl ether methacrylate]s (P(OEG)MAs) are synthesized from commercial macromonomers, these are structurally polydisperse, as OEG segments feature a broad distribution of lengths. Herein, we investigate the influence of side-chain heterogeneity on Li-ion transport by comparing structurally polydisperse P(OEG)MAs with analogous graft polymers with homogeneous architecture, generated from discrete macromonomer feeds obtained through flash chromatography. Ionic conductivity was found to increase with increasing side-chain dispersity. For structurally polydisperse P(OEG)MAs, enhancing side-chain heterogeneity resulted in greater salt dissociation and higher ionic conductivity at relatively high salt contents. These trends are uncorrelated with differences in thermal properties, rheology, and polymer diffusivity, indicating that ion transport is not governed by overall polymer dynamics. Dispersity of side chains thus emerges as a determinant for Li-ion transport in PEs based on P(OEG)MAs. However, this effect is lost when backbone flexibility increases, i.e., when polymethacrylates are substituted with more flexible polyacrylate counterparts. By elucidating how side-chain heterogeneity and backbone flexibility affect ion transport, this work provides guidance for the rational design of graft PEs.

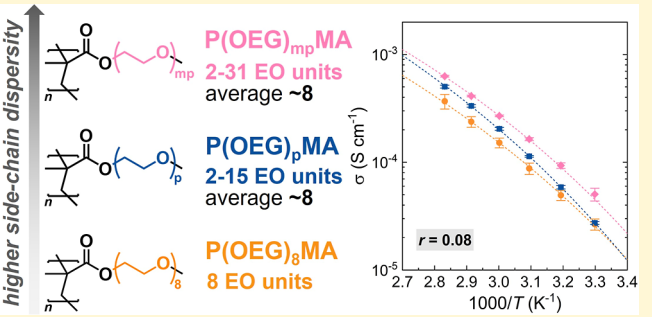

Downloaded via 151.44.39.40 on May 11, 2026 at 20:13:35 (UTC).
See https://pubs.acs.org/sharingguidelines for options on how to legitimately share published articles.

1. INTRODUCTION

Polymer electrolytes (PEs) are key materials for high-energy-density electrochemical energy storage. For decades, polyethers—and especially poly(ethylene oxide) (PEO)—have attracted continued interest due to their superior ability to solvate and transport alkali-metal cations. However, the inherent limitations of PEO—primarily arising from its semicrystalline nature—have prompted efforts to improve the electrochemical performance of polyether-based PEs.[1−3] Several structural parameters, such as end-functionalities and molecular weight, have been extensively studied to elucidate their effects on ion transport.

Dispersity of polymer molar mass ($Đ$) plays a critical role in various properties of polymeric materials, including viscosity, processability, and thermal and mechanical behavior.[4−7] While dispersity has been exploited to tailor polymer self-assembly in bulk and in solution and tune the mechanical properties of networks and elastomeric materials,[8] its impact on ion transport in PEs has been rarely considered. Mahanthappa et al. synthesized a series of polystyrene(PS)-*b*-PEO-*b*-PS triblock copolymers with different $Đ$ of the PEO block.[9,10] They measured an enhancement in ionic conductivity with increasing $Đ$, which was attributed to smaller lamellar grain size in copolymers with more disordered PEO blocks, resulting in improved intergrain connectivity and ion transport. Watanabe et al. compared the ionic conductivities and mechanical properties of various network polymer electrolytes including a homogeneous model network composed of 4-arm poly(ethylene glycol) (tetra-PEG).[11,12] They found that the average network size played a more significant role than the mesh size distribution in governing ion transport, although the homogeneous network exhibited superior toughness.

Graft polymers bearing oligo(ethylene glycol) (OEG) side chains hold promise as components of PEs.[1,13−16] Their relatively short oligoether side chains provide polymers with reduced crystallinity compared with PEO, resulting in enhanced ionic conductivity at lower temperatures. Moreover, the design space of macromonomers with OEG side chains is vast.[17−23] Their polymerization can be achieved through

Received: December 23, 2025
Revised: January 28, 2026
Accepted: February 2, 2026
Published: February 6, 2026

© 2026 The Authors. Published by American Chemical Society

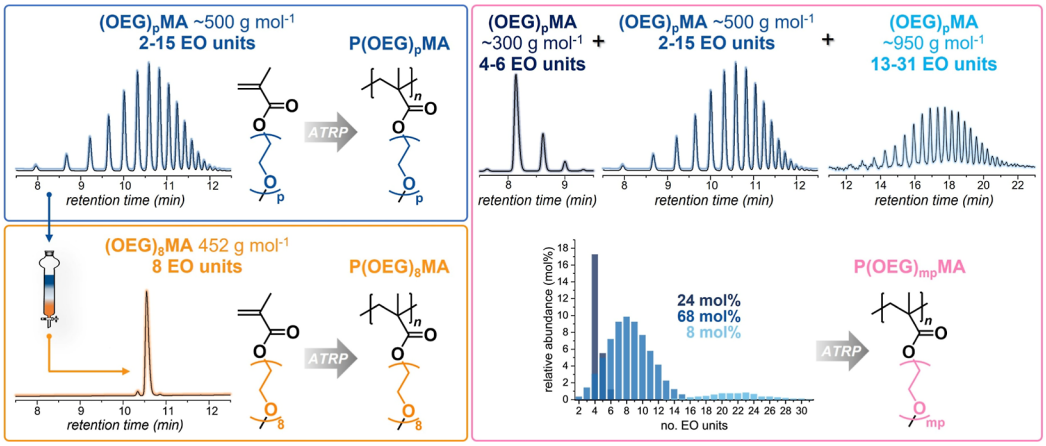

Figure 1. Chemical structure and UPLC elugrams of the commercial macromonomers $(OEG)_pMA$-300, $(OEG)_pMA$-500, and $(OEG)_pMA$-950 (with M_n ~ 300, ~500, and ~950 g mol^{-1}) and the discrete $(OEG)_8MA$ separated by flash chromatography from $(OEG)_pMA$-500. Chemical structure of the polymers derived from $(OEG)_8MA$, $(OEG)_pMA$-500, and the macromonomers' mix giving a polymer with increased side-chain heterogeneity, i.e., $P(OEG)_{mp}MA$.

various techniques, including ionic polymerizations and reversible deactivation radical polymerizations, enabling control over (co)polymer architecture and composition.[13,24] A common—yet often overlooked—feature of these macromonomers is that they typically present a distribution of OEG side-chain lengths rather than a discrete number of ethylene oxide (EO) units. The extent to which this intrinsic structural dispersity influences ion transport remains unexplored.

Recent works have shown that the dispersity of OEG side chains can serve as a synthetic tool to manipulate various polymer properties.[25−29] Lawrence et al. reported that uniform bottlebrushes featuring discrete backbone and OEG side chains and a fluorinated terminus outperform their heterogeneous counterparts as ^{19}F MRI contrast agents.[25] Our group demonstrated that poly[oligo(ethylene glycol) methyl ether methacrylate] (P(OEG)MA) brushes comprising uniform OEG side chains exhibit increased hydration, lubricity, and colloidal stability in comparison with parent brushes bearing a distribution of side-chain lengths.[26,27]

Aiming to assess the influence of structural dispersity on Li-ion transport, we synthesized poly(meth)acrylates with discrete and variably disperse OEG side chains and blended them with lithium bis(trifluoromethanesulfonyl)imide (LiTFSI). The thermal and rheological properties, polymer and ion diffusivity, and conductivity of these PEs were investigated and correlated with the structural features of the polymers.

Previous experimental and theoretical studies on P(OEG)MA-based PEs revealed that the length of OEG side chains is the main factor determining Li-ion conductivity.[21,30] This behavior was attributed to heterogeneous polymer dynamics resulting from the graft architecture. The EO units close to the relatively immobile backbone show slow relaxations, whereas those farther from the backbone participate much more effectively in Li-ion solvation, determining the overall conductivity. In this work, we show that P(OEG)MA-based PEs display higher ionic conductivity as the heterogeneity of side-chain lengths increases. This effect becomes less significant for analogous polyacrylates that feature a more flexible backbone. For more rigid polymethacrylate backbones, broadening the distribution of the OEG side-chain lengths enables us to introduce relatively long chains which, on the one hand, increase polymer−polymer and polymer−ion interactions and, on the other hand, improve ion transport. By enhancement of the dispersity of the OEG side chains relative to a commercial (OEG)MA macromonomer, it is possible to increase the content of Li salt in the corresponding PE while maintaining high salt dissociation and conductivity. Thus, structural dispersity emerges as a complementary design parameter—alongside side-chain length and composition—for optimizing the ion transport properties of graft polymer electrolytes.

2. RESULTS AND DISCUSSION

Commercially available (OEG)MA macromonomers are mixtures of methacrylates bearing OEG side chains with varying degrees of polymerization. We focused on the commercial macromonomer with an average molar mass of ~500 g mol^{-1} ($(OEG)_pMA$-500, where "p" stands for "polydisperse" to account for the presence of multiple species). This choice was motivated by several factors: (i) PEs based on $(OEG)_pMA$-500 exhibit higher ionic conductivity (σ) than those based on $(OEG)_pMA$ with M_n ~ 300 g mol^{-1} ($(OEG)_pMA$-300);[21] (ii) the higher crystallinity[31] of $(OEG)_pMA$ with M_n ~ 950 g mol^{-1} ($(OEG)_pMA$-950) compared to $(OEG)_pMA$-500 can be detrimental for Li-ion transport; (iii) the entanglement molecular weight of PEO is ~1−2 kg mol^{-1},[22,32] making $P(OEG)_pMA$ with longer side chains more likely to form entanglements that reduce Li-ion mobility, particularly at room temperature.

A combination of ultraperformance liquid chromatography (UPLC) and high-performance LC coupled with electrospray ionization mass spectrometry (HPLC-ESI/MS) revealed that $(OEG)_pMA$-500 featured a distribution of OEG side chains ranging from 2 to 15 EO units (Figures 1 and S1 and Table S1).[26] This determines a calculated number-average molar mass $M_{n,calc}$ = 466 ± 117 g mol^{-1} and dispersity $Đ$ = 1.06 (Table S2). The most abundant species (14.6 mol %) features 8 EO units in the side chain, i.e., $(OEG)_8MA$ (molar mass of 452 g mol^{-1}). Flash silica gel chromatography was employed to isolate the discrete species $(OEG)_8MA$ in good yield (~60%).[26,33] HPLC-ESI/MS analysis of the discrete macromonomer sample revealed the presence of traces of $(OEG)_7MA$ and $(OEG)_9MA$, while $(OEG)_8MA$ accounted for 98.5 mol % (Figures 1 and S2 and Tables S3 and S4),

https://doi.org/10.1021/acs.chemmater.5c03475
Chem. Mater. 2026, 38, 2063−2071

Table 1. Structural Parameters, T_g, and Ionic Conductivity (σ) of Poly(meth)acrylates with Discrete and Disperse OEG Side Chains

polymer	M_n[a] (kg mol^{-1})	$Đ$[a]	T_g (°C)	$T_{g,r=0.08}$ (°C)	$\sigma_{r=0.08,50\ °C}$[b] (10^4 S cm^{-1})	$\sigma_{r=0.05,50\ °C}$[b] (10^4 S cm^{-1})	E_a (kJ mol^{-1})
P(OEG)$_8$MA	26.9	1.44	−62	−47	0.88 ± 0.11	1.32 ± 0.06	9.89 ± 0.16
P(OEG)$_p$MA	29.1	1.35	−61	−40	1.14 ± 0.02	1.69 ± 0.15	10.07 ± 0.06
P(OEG)$_{mp}$MA	27.3	1.41	−65	−39	1.64 ± 0.06	1.79 ± 0.25	8.78 ± 0.17
P(OEG)$_8$A	33.5	1.15	−64	−47	2.49 ± 0.02	3.09	9.44 ± 0.07
P(OEG)$_p$A	32.5	1.18	−63	−45	2.53 ± 0.11	2.94	9.04 ± 0.11

[a]Measured by GPC in DMF + 0.01 M LiBr as eluent, using poly(methyl methacrylate) standards. [b]For polymethacrylate-based electrolytes, conductivity values are reported as the average of measurements on different polymers with similar structural and thermal characteristics (the polymer library is reported in Table S8).

resulting in $M_{n,calc}$ = 452 ± 5 g mol^{-1} and dispersity $Đ$ = 1.00014 (hereafter approximated as $Đ$ = 1.00). ^{1}H NMR spectra of (OEG)$_p$MA-500 and (OEG)$_8$MA showed an average number of EO units $n_{av,EO}$ = 8.7 and 8.2 (Figures S3 and S4).

The corresponding polymers with discrete and heterogeneous OEG side chains, P(OEG)$_8$MA and P(OEG)$_p$MA, were prepared by activators regenerated by electron transfer atom transfer radical polymerization (ARGET ATRP, Figures S3−S6). Different batches of the two polymers were prepared under identical polymerization conditions to enable statistically robust characterizations. Purified polymers showed M_n values of 20−29 kg mol^{-1} and main-chain $Đ$ = 1.3−1.4 (Figures S9 and S10 and Table S8). ^{1}H NMR spectra revealed $n_{av,EO}$ = 8.8 and 8.2 for P(OEG)$_p$MA and P(OEG)$_8$MA, respectively (Figures S12 and S13), identical with the corresponding macromonomers.

Additionally, we reasoned that the heterogeneity of the OEG side chains could be intentionally enhanced by mixing (OEG)$_p$MA macromonomers with different OEG side-chain distributions to form P(OEG)$_{mp}$MA, where "mp" stands for "more polydisperse". Commercial (OEG)$_p$MA-300 and (OEG)$_p$MA-950 were also analyzed by UPLC and HPLC-ESI/MS (Figure 1 and Table S1). (OEG)$_p$MA-300 showed a rather narrow distribution of species, with $M_{n,calc}$ = 291 ± 25 g mol^{-1} and $Đ$ = 1.01. In contrast, (OEG)$_p$MA-950 comprised at least 19 different species with 13−31 EO units in the side chain, resulting in $M_{n,calc}$ = 1056 ± 169 g mol^{-1} and $Đ$ = 1.03. Thus, we prepared a macromonomer mixture comprising 24, 68, and 8 mol % of (OEG)$_p$MA-300, (OEG)$_p$MA-500, and (OEG)$_p$MA-950, respectively. The mixture has $M_{n,calc}$ = 471 ± 217 g mol^{-1} and $n_{av,EO}$ = 8.5 (Table S5), comparable with (OEG)$_p$MA-500 and (OEG)$_8$MA. However, $Đ$ = 1.21, which is substantially larger than the dispersity of (OEG)$_p$MA-500 ($Đ$ = 1.06) and of the discrete (OEG)$_8$MA ($Đ$ = 1.00).

P(OEG)$_{mp}$MA was generated by ARGET ATRP of the macromonomer mixture, reaching nearly quantitative conversion to ensure the incorporation of all different (OEG)MAs into the polymer (Table 1). P(OEG)$_{mp}$MA samples exhibited M_n = 27 kDa, main-chain $Đ$ = 1.3−1.4 (Table S8 and Figure S11), and $n_{av,EO}$ = 8.8, according to ^{1}H NMR analysis (Figure S14).

The thermal properties of P(OEG)$_8$MA, P(OEG)$_p$MA, and P(OEG)$_{mp}$MA were measured by differential scanning calorimetry (DSC, Figure 2) and thermogravimetric analysis (TGA, Figure S24). The polymers showed no substantial difference in glass transition and decomposition temperatures (T_gs of approximately −62 °C, and T_ds ~ 370 °C, respectively, Tables S9). The polymer with discrete side chains, P(OEG)$_8$MA, exhibited a completely amorphous character, as

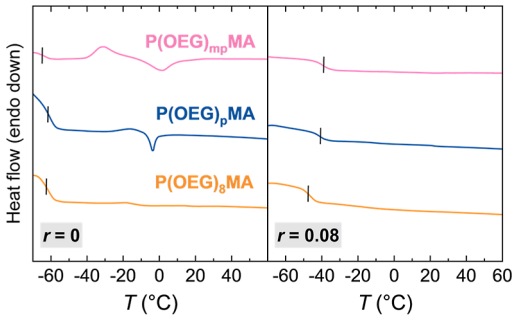

Figure 2. DSC thermograms (heating ramp) of P(OEG)MAs without (r = 0) and with added LiTFSI (r = [Li$^+$]/[EO] = 0.08). Curves are vertically offset for clarity. Vertical lines indicate glass transition temperatures.

relatively short side chains prevent the formation of ordered domains.[22,29] For the polymers with heterogeneous side chains, no crystallization occurred during the cooling stage; however, cold crystallization transitions were detected at T_{cc} = −21 and −31 °C for P(OEG)$_p$MA and P(OEG)$_{mp}$MA, respectively (Figure 2). The cold crystallization phenomenon was previously reported for P(OEG)MAs with discrete side chains bearing 9 and 10 EO units, and T_{cc} values decreased with increasing the number of EO units.[29] For P(OEG)$_p$MA, this transition is partially coupled with melting (T_m = −4 °C), whereas for P(OEG)$_{mp}$MA, it is more distinct, although both the exothermic and melting peaks (T_m = 3 °C) are rather broad. While side-chain heterogeneity limits the ordering of polymer chains,[29] the presence of relatively long side chains in P(OEG)$_{mp}$MA favors the formation of ordered arrangements.

PEs were prepared by blending each polymer with LiTFSI. The molar ratio of EO units to Li ions was initially fixed at r = [Li$^+$]/[EO] = 0.08, considering that the highest conductivity of PEO-based electrolytes is typically measured for r = 0.05−0.08.[22,34] The introduction of Li salt resulted in an increase in the T_g compared to neat polymers (Table 1 and Figure 2). This behavior is typical of PEO-based PEs where associations between ions and polymer segments slows down the segmental relaxations of polymer chains.[20,35] Additionally, no melting peak was detected for all PEs (Table S9), indicating that the coordination of Li$^+$ to ether oxygens disrupts the alignment of OEG side chains in P(OEG)$_p$MA and P(OEG)$_{mp}$MA, thereby suppressing crystallization.[20,36] PEs based on P(OEG)$_8$MA showed T_g values that were 7−8 °C lower than those of PEs with heterogeneous OEG side chains. Previous works highlighted that the addition of Li salt tends to raise T_g to a greater extent for polymers with shorter OEG side chains, which are more prone to undergo interchain cross-links than intrachain cross-links.[17,20] Thus, the observed difference in T_g might

https://doi.org/10.1021/acs.chemmater.5c03475
Chem. Mater. 2026, 38, 2063−2071

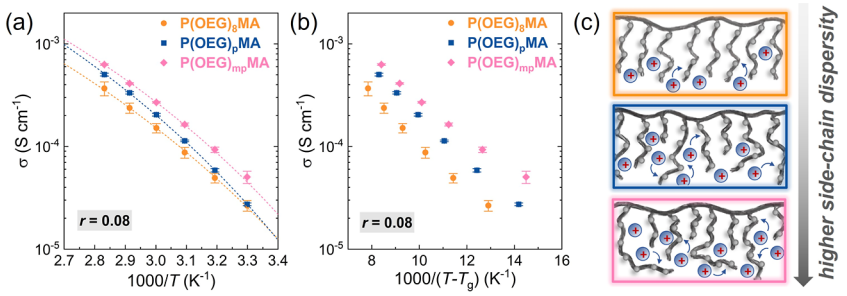

Figure 3. Ionic conductivity (σ) measured by EIS (a) and corrected by T_g (b) of PEs comprising LiTFSI (r = [Li$^+$]/[EO] = 0.08) and polymethacrylates with discrete and disperse OEG side chains. In (a), σ values were fitted using the Vogel−Tammann−Fulcher (VTF) equation, where the Vogel temperature $T_0 = T_g - 50$ K. (c) Cartoon illustrating the distribution of OEG side chains in the PEs and their interactions with Li ions.

originate from the presence of relatively short side chains in P(OEG)$_p$MA and P(OEG)$_{mp}$MA, which are absent in P(OEG)$_8$MA.

The ionic conductivity (σ) of PEs (r = 0.08) was measured by electrochemical impedance spectroscopy (EIS) in a temperature range of 30−80 °C, with 10 °C intervals (Figure 3a). The ionic conductivity increased with an increase in the dispersity of the OEG side chains at nearly all temperatures. PEs based on P(OEG)$_8$MA and P(OEG)$_p$MA showed similar σ values at ambient temperature; however at $T \geq 50$ °C, the PE with discrete OEG side chains showed consistently lower conductivity. At 50 °C, the σ value of P(OEG)$_8$MA fell below the common benchmark for PEs of 0.1 mS cm^{-1}. Within the explored temperature range, PE featuring the broadest distribution of side-chain lengths, P(OEG)$_{mp}$MA, displayed σ values approximately twice those of P(OEG)$_8$MA and 1.5 times higher than those of P(OEG)$_p$MA (Table 1).

For each P(OEG)MA, conductivity measurements were performed on at least three independently prepared samples, using different polymer batches (Table S8) and freshly prepared LiTFSI blends each time. The relatively small error bars reported in Figure 3a indicate that variations in molar mass, main-chain dispersity, and sample preparation have a negligible effect on ion-transport properties, whereas side-chain dispersity is the primary descriptor for these PEs.

Temperature-dependent conductivity data for all PEs were fitted using the Vogel−Tammann−Fulcher (VTF) equation:

$$\sigma = Ae^{\frac{-E_a}{R(T-T_0)}} \quad (1)$$

where E_a is the pseudoactivation energy, A is a constant prefactor, and T_0 is the Vogel temperature, defined as $T_0 = T_g - 50$ K.[37] VTF fit parameters are shown in Tables 1 and S10. For all PEs, the variation of σ with temperature followed VTF behavior, indicating that ion transport is assisted by the dynamics of the polymer matrix, as typical of PEs above their T_g. To account for the different T_g values of the PEs, σ values were plotted as a function of $(T-T_g)^{-1}$ (Figure 3b). In this plot, all points overlap for different PEs if the differences in their ionic conductivities are governed by variations in segmental motion, which are sufficiently described by the T_g.[21,38] Thus, the plot in Figure 3b highlights that the average segmental dynamics expressed by T_g cannot fully explain the different ionic conductivities of P(OEG)MAs with varied side-chain distributions.

Bennington et al. have demonstrated that trends in ionic conductivity for similar P(OEG)$_p$MAs synthesized from (OEG)$_p$MA-300 and (OEG)$_p$MA-500 are primarily governed by side-chain length, which outweighs the effect of T_g.[21] As the EO units located far from the backbone display increased segmental dynamics, they are more effective in promoting ion transport, leading to higher σ values for P(OEG)$_p$MA with longer side chains. Of note, ∼25 mol % of the species in (OEG)$_p$MA-500 have side chains with the same or lower number of EO units than those found in (OEG)$_p$MA-300 (4−6 units, Table S1) and therefore do not effectively contribute to the conductivity enhancement. MD simulations of graft polymethacrylates with 9 side-chain EO units have revealed that units 4−9 (with 9 being the farthest from the backbone) are the most frequently involved in Li$^+$ solvation. However, the side-chain heterogeneity of common P(OEG)$_p$MAs was not considered in simulations, thus neglecting the influence of EO units located even further from the backbone.

In the P(OEG)$_p$MA used in this work, nearly half (∼46%, Table S1) of the repeating units have >8 EO segments. Thus, in comparison to P(OEG)$_8$MA, P(OEG)$_p$MA possesses a greater proportion of EO units that effectively participate in ion solvation (Figure 3c). At the same time, a smaller fraction (∼40%) of the repeating units in P(OEG)$_{mp}$MA have >8 EO segments, yet approximately one-sixth of those contain more EO units than the longest side chains of P(OEG)$_p$MA (i.e., >15 EO units). The presence of such long side chains (Figure 3c) likely plays a major role in enhancing the conductivity of P(OEG)$_{mp}$MA.

Additionally, the longer side chains in P(OEG)$_{mp}$MA are rather diluted, which may further enhance their mobility and involvement in the solvation site formation. Ji et al. reported that OEG side-chain dilution by copolymerization of (OEG)$_p$MAs with methyl methacrylate (MMA) generally determines a decrease in ionic conductivity, due to disruption of solvation site connectivity.[22] However, MMA has a poor Li-ion coordination ability and slow dynamics, thus negatively impacting σ. Conversely, the manipulation of the OEG side-chain dispersity allows for diluting longer side chains comprising a greater proportion of highly mobile EO units with shorter side chains still capable of promoting Li-ion transport, albeit to a lower extent. Furthermore, broadening side-chain distribution while keeping a constant $n_{av,EO}$ of approximately 8 limits the increase in crystallinity caused by the use of P(OEG)$_p$MAs with longer side chains.[22]

To support the hypothesis that the presence of long chains is critical for enhancing the ionic conductivity of these graft PEs, we prepared a polymer using a macromonomer mixture composed primarily of (OEG)$_p$MA-300 (75 mol %), with the addition of 23 mol % (OEG)$_p$MA-950 and 2 mol %

https://doi.org/10.1021/acs.chemmater.5c03475
Chem. Mater. 2026, 38, 2063−2071

$(OEG)_pMA$-500 to maintain $n_{av,EO}$ = 8.5. The ionic conductivity of the corresponding PE was an order of magnitude higher than that of an analogous PE composed exclusively of $(OEG)_pMA$-300[21,22] and was comparable to that of $P(OEG)_pMA$ (i.e., composed exclusively of $(OEG)_pMA$-500, Figure S25).

Aiming to understand whether the enhanced ion transport promoted by side-chain heterogeneity is influenced by the flexibility of the polymer backbone, we synthesized polyacrylates with tailored side-chain-length distributions. Analogously to $(OEG)_pMA$, (oligo ethylene glycol) methyl ether acrylate with $M_n \sim 480$ g mol^{-1}, $(OEG)_pA$-480, comprises species with varying number of EO units in the side chains. UPLC and HPLC-ESI/MS revealed a similar side-chain distribution to that of $(OEG)_pMA$-500, with EO units ranging from 3 to 15, $M_{n,calc}$ = 461 ± 117 g mol^{-1}, and the highest abundance (16 mol %) of the macromonomer with 8 EO lateral segments, $(OEG)_8A$ (Tables S6 and S7 and Figure S15). Upon separation of $(OEG)_8A$ by flash chromatography, the polyacrylates with discrete and disperse OEG side chains, $P(OEG)_8A$ and $P(OEG)_pA$, were synthesized by ARGET ATRP. The two polymers featured similar M_n of ∼33 kDa, $Đ$ < 1.2 (Table 1 and Figure S22), and $n_{av,EO}$ = 8.3 and 8.8 for $P(OEG)_8A$ and $P(OEG)_pA$, respectively (Figures S20 and S21).

The temperature-dependent ionic conductivity of the polyacrylate-based PEs (r = 0.08) is shown in Figure 4. In

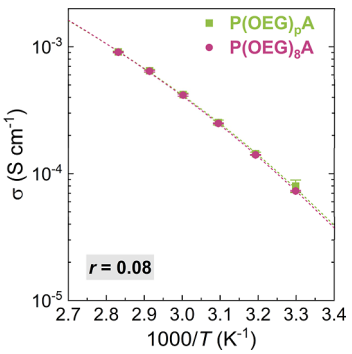

Figure 4. Ionic conductivity (σ) values measured by EIS of PEs comprising LiTFSI (r = [Li$^+$]/[EO] = 0.08) and polyacrylates with discrete and disperse OEG side chains. σ values were fitted using the VTF equation, where the Vogel temperature $T_0 = T_g - 50$ K.

contrast to P(OEG)MAs, P(OEG)A-based electrolytes exhibited no appreciable effect of side-chain dispersity on σ values. At the same time, at T = 50 °C, σ more than doubled compared to that of $P(OEG)_pMA$, in agreement with the measurements of Bennington et al.[21] This difference in conductivity is not captured by the polymers' T_g (Tables 1 and S8) but rather originates from the higher flexibility of polyacrylates' backbone in comparison with polymethacrylates. The faster relaxation of polyacrylates' backbone leads to more rapid relaxation of the EO units in its proximity than in the corresponding polymethacrylates.[21] Thus, we primarily attribute the negligible influence of side-chain dispersity to accelerated backbone relaxation, which minimizes the position dependence of EO segmental dynamics.

To gain further insight into the relations between side-chain dispersity, polymer mobility, and ion transport, the viscoelastic response of P(OEG)MAs and the corresponding PEs was studied by oscillatory rheometry in the linear regime (strain 1%) at 25 °C. Neat $P(OEG)_8MA$ and $P(OEG)_pMA$ exhibited "liquid-like" viscoelastic behavior, with the gap between G'' and G' decreasing at higher frequency (Figure S26). For neat $P(OEG)_{mp}MA$, G' showed a weak dependence on frequency and it was higher than G'' at relatively low frequencies, indicating an elastic behavior, which is attributed to the interpenetration of longer chains. Upon addition of salt (r = 0.08) to $P(OEG)_{mp}MA$, G' shows a more pronounced frequency dependence and greater values at relatively high frequencies, as salt interactions enhance the elasticity of polymer chains.[39] In the explored frequency range, $G'' > G'$ denotes a liquid-like behavior. For all PEs, an increase in G'' is observed upon addition of salt, as polymer−salt interactions increase the viscosity of the materials. $P(OEG)_{mp}MA$ showed the highest values of G'' in the analyzed frequency range.

Structural differences and dynamics of P(OEG)MAs were further probed by ^{1}H high-resolution nuclear magnetic spectroscopy (HR NMR), in the temperature range of 25−84 °C. For all P(OEG)MAs blended with LiTFSI (r = 0.08), broad resonances were recorded at 25 °C, which narrowed significantly with increasing the temperature as a consequence of enhanced chain mobility (Figure S27). To obtain sharper lines, ^{1}H HR-magic angle spinning (HR-MAS) spectra were acquired for both neat polymers and their blend with LiTFSI. The spectra showed well-resolved peaks even at 25 °C for all neat P(OEG)MAs (Figure S28). The addition of salt caused a slight downfield shift of the peak associated with the methylene protons in EO units.[40] Moreover, a new peak appeared for all polymers at 4.01−4.15 ppm, which is likely associated with the $-CH_2$ close to the ester group in EO unit 1. Interestingly, at 65 °C, $P(OEG)_8MA$ showed sharp peaks, which were broader for $P(OEG)_pMA$ and for $P(OEG)_{mp}MA$ (Figure S29). This trend indicates that $P(OEG)_8MA$ chains remain highly mobile upon introduction of Li salt, whereas mobility decreases for the polymers with heterogeneous side chains.

The longitudinal (spin−lattice, T_1) relaxation time for protons, providing information about their rotational mobility, are reported in Table S11. The T_1 lowest values are obtained for $P(OEG)_{mp}MA$ and its corresponding PE. We hypothesize that this relatively fast short-range rotational motion originates from the high proportion of short (4−6 EO units) side chains in $P(OEG)_{mp}MA$. Pulsed-gradient spin−echo (PGSE) NMR experiments were conducted to measure the diffusion coefficients (Ds) of the neat polymers and their blends with LiTFSI. $P(OEG)_8MA$ exhibited the higher value of D in comparison with the other polymers (Table S12), suggesting that the interdigitation of relatively long chains in $P(OEG)_pMA$ and $P(OEG)_{mp}MA$ hinders the translational motion of the polymers. The addition of Li-salt resulted in nearly unchanged or lowered D values, due to Li$^+$ coordination that slows down segmental motion.

Rheological and diffusivity studies thus indicated that P(OEG)MAs with enhanced side-chain heterogeneity show higher viscosity and polymer−polymer and polymer−ion interactions than $P(OEG)_8MA$. This is reflected in the lower T_g of $P(OEG)_8MA$ blended with LiTFSI. The opposite trend measured for ionic conductivity, with σ values increasing with side-chain heterogeneity, indicates that overall polymer dynamics do not effectively account for ion transport in graft PEs, in agreement with the findings of Bennington et al.[21]

PEs with different contents of Li salt (r = 0.02, 0.05, and 0.1) were also prepared and their conductivity was measured at T ranging from 30 to 80 °C (Figures 5a and S30 and Table

https://doi.org/10.1021/acs.chemmater.5c03475
Chem. Mater. 2026, 38, 2063−2071

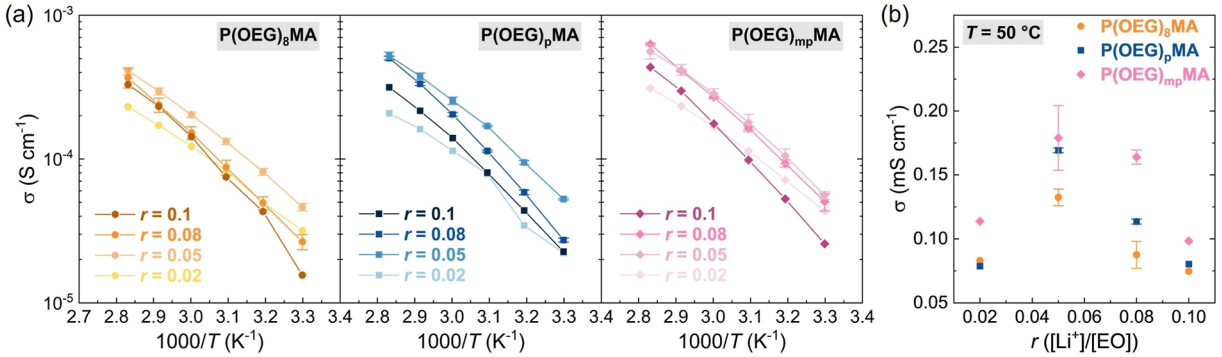

Figure 5. (a) Variation of ionic conductivity (measured by EIS) with the amount of LiTFSI (expressed as r = [Li$^+$]/[EO]) for PEs based on polymethacrylates with discrete and increasingly more disperse OEG side chains. (b) Comparison of σ values as a function of r for the different PEs at T = 50 °C.

S13). All PEs exhibited the typical trend for PEO-based electrolytes, whereby σ increases with increasing r up to a threshold value beyond which the high content of Li$^+$ forming cross-links among chains strongly diminishes their mobility and reduces free volume, hindering intrachain and interchain hopping.[41] For P(OEG)$_8$MA and P(OEG)$_p$MA, σ at r = 0.08 is lower than that at r = 0.05, particularly at relatively low temperatures. In contrast, P(OEG)$_{mp}$MA with r = 0.05 and 0.08 showed similar σ values at all temperatures, and the effect of excessive cross-linking became evident only at r = 0.1 (Figure 5). Moreover, P(OEG)$_{mp}$MA exhibited σ values higher than those of the PEs with less heterogeneous side chains at all r values (Figure 5b). In contrast, P(OEG)$_8$A and P(OEG)$_p$A exhibited very similar σ values at all salt contents and temperatures (Figure S30).

At r = 0.05, P(OEG)MAs showed higher ionic conductivity than reported literature values for PEO at T < 50 °C.[21,30] In particular, P(OEG)$_p$MA and P(OEG)$_{mp}$MA exhibited approximately 2- and 3-fold higher σ values, respectively, compared to PEO (with M_n above its entanglement molecular weight) at T = 30 °C, underscoring the advantages of employing graft PEs for room-temperature applications.

To further elucidate the influence of the OEG side-chain dispersity on ion transport, we used ^{7}Li and ^{19}F pulsed gradient spin echo (PGSE) NMR to measure the self-diffusion coefficients of Li$^+$ and TFSI$^-$ ions, respectively, in the temperature range of 30−80 °C for P(OEG)$_p$MA and P(OEG)$_{mp}$MA with r = 0.08 (Figures 6 and S31). While D_{anion} was very similar for both PEs, D_{cation} was slightly higher for P(OEG)$_p$MA. This is consistent with rheological data showing enhanced polymer−ion interactions for the polymer with more heterogeneous side chains. The negligible influence of polymer structure on D_{anion} indicates that polymer chains are predominantly interacting with Li ions.[42]

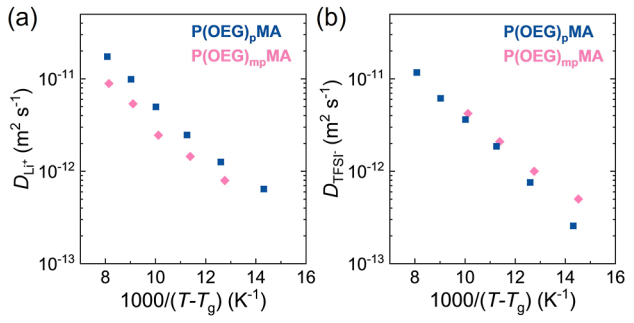

Figure 6. Diffusion coefficients of (a) Li$^+$ (^{7}Li) and (b) TFSI$^-$ (^{19}F) as a function of reduced temperature (T−T_g), measured by PGSE NMR across the temperature range 25−84 °C for P(OEG)$_p$MA- and P(OEG)$_{mp}$MA-based electrolytes with r = 0.08.

The activation energy for cation and anion diffusion ($E_{a,diff}$) was determined by fitting the temperature dependence of the diffusion coefficients to the Arrhenius equation:

$$D(T) = D_0 \exp\left(-\frac{E_a}{RT}\right) \quad (2)$$

where D_0 is a pre-exponential factor (Figure S31). The $E_{a,diff}$ values for the diffusion of TFSI$^-$ were 62.2 ± 4.5 and 60.0 ± 1.1 kJ mol^{-1} for P(OEG)$_p$MA and P(OEG)$_{mp}$MA, respectively, whereas for Li$^+$ diffusion, $E_{a,diff}$ = 55.8 ± 1.1 and 51.2 ± 2.2 kJ mol^{-1} for P(OEG)$_p$MA and P(OEG)$_{mp}$MA, respectively. For both PEs, the activation energy associated with TFSI$^-$ diffusion is higher than that of Li$^+$, which can be attributed to the distinctive transport mechanism of Li$^+$ ions, whose motion is coupled to the segmental dynamics of the polymer matrix.[36]

The self-diffusion coefficients of Li$^+$ and TFSI$^-$ ions can be used to estimate the inverse Haven ratio, which is typically interpreted as the degree of dissociation (α) of the Li salt.[42−44] This is obtained by comparing σ measured by EIS to the conductivity calculated by the Nernst−Einstein equation (eq 3), using D_{cation} and D_{anion} measured by NMR:

$$\sigma_{NMR} = \frac{F^2}{RT} \sum c_i z_i D_i \quad (3)$$

where c_i is the molar concentration of the ions, z_i is their absolute charge, D_i is their diffusion coefficient, and F is the Faraday constant. Thus, the Nernst−Einstein equation provides conductivity values in the ideal case of complete salt dissolution and absence of ion aggregation, i.e., when all species contributing to ion self-diffusion are also responsible for measured conductivity values.[43,45] The degree of salt dissociation is then defined as $\alpha = \sigma/\sigma_{NMR}$. Values of α below unity are common in PEs, and they are attributed to neutral ion pairs that do not contribute to conductivity under an applied electric field, but their motion contributes to the diffusion coefficients measured by NMR.[43] Relevantly, P(OEG)$_{mp}$MA showed α = 0.84−1, whereas P(OEG)$_p$MA exhibited a lower value of α = 0.50−0.64 (Table S14). Thus, LiTFSI is substantially more dissociated in the polymer with more heterogeneous OEG side chains. As the salt content is increased in PEs, ion aggregation also tends to increase.[46,47]

https://doi.org/10.1021/acs.chemmater.5c03475
Chem. Mater. 2026, 38, 2063−2071

However, LiTFSI remained largely dissociated for P-(OEG)$_{mp}$MA at r = 0.08, contributing to maintaining relatively high conductivity values.

3. CONCLUSION

The role of structural dispersity in graft PEs bearing EO units in their side chains was investigated. PEs with uniform side chains ($Đ$ = 1.00) were synthesized by isolating discrete (meth)acrylate macromonomers with 8 EO units in the lateral segments. To broaden the distribution of side-chain length in P(OEG)MAs, macromonomers with different compositions were blended to obtain a side-chain dispersity of $Đ$ > 1.2.

Ionic conductivity increased with an increase in the heterogeneity of the OEG side chains in graft polymethacrylate electrolytes. This trend was not paralleled by similar variations in T_g or polymer diffusivity, indicating that overall polymer dynamics have a limited influence on ion transport. The presence of relatively long side chains in P(OEG)MAs with higher heterogeneity provides a large fraction of EO units that effectively participate in ion solvation, determining higher σ values. Additionally, long side chains are diluted along the backbone by shorter, yet ion-coordinating, side chains, which limits their tendency to crystallize without penalizing conductivity through the introduction of noncoordinating spacer moieties. These effects, however, become negligible in analogous polyacrylate electrolytes, in which the local dynamics of EO units are overridden by the enhanced flexibility of the backbone.

For more rigid polymethacrylate electrolytes, the polymer with the highest side-chain heterogeneity, P(OEG)$_{mp}$MA, enabled greater dissociation of Li salt and thus maintained high σ values when increasing the salt content from r = 0.05 to r = 0.08, whereas other PEs showed a marked decrease in conductivity.

The dominant effect of local EO-unit dynamics, rather than overall polymer dynamics, on ion transport in P(OEG)MAs makes side-chain heterogeneity a key structural feature. These findings thus show that structural dispersity of graft polymers can be used as a tool to modulate ion transport and ultimately design PEs with improved performance.

4. METHODS

4.1. Isolation of Discrete (OEG)$_8$MA and (OEG)$_8$A

(OEG)$_p$MA was dissolved in the eluent (98/2 EtOAc/MeOH), and (OEG)$_8$MA was isolated by flash chromatography using silica gel under nitrogen pressure. Single-fraction detection was performed using SiO_2-coated TLC sheets stained with a $KMnO_4$ solution and the previously mentioned mobile phase. Solutions of discrete macromonomer fractions were dried in a rotavapor under reduced pressure after the addition of hydroquinone, which acts as an inhibitor. Both commercial macromonomers and (OEG)$_8$MA were characterized by ^{1}H NMR and UPLC and stored at −20 °C. The same procedure was used to isolate (OEG)$_8$A from (OEG)$_p$A.

4.2. Polymerization of (OEG)MAs and (OEG)As

P(OEG)$_8$MA, P(OEG)$_p$MA, P(OEG)$_{mp}$MA, and P(OEG)$_X$MA were synthesized by activators regenerated by electron transfer atom transfer radical polymerization (ARGET-ATRP). In a representative polymerization, $CuBr_2$ (22.3 mg, 0.10 mmol) and TPMA (32.3 mg, 0.11 mmol) were dissolved in 2 mL of DMF. Then, (OEG)$_8$MA (1.07 g, 2.37 mmol), Milli-Q H_2O (3.96 mL), HEBiB (5 μL, 0.03 mmol), NaBr (23.1 mg, 0.23 mmol), and 0.13 mL of the solution of $CuBr_2$/tris(2-pyridylmethyl)amine (TPMA) were added into a Schleck flask. The solution was degassed with Ar for 30 min. Separately, L-ascorbic acid (AscAc, 26.4 mg, 0.15 mmol) was dissolved in 5 mL of Milli-Q H_2O in a round-bottom flask, and the solution was degassed with Ar for 30 min. To start the polymerization, 35 mL (0.15 equiv relative to $CuBr_2$) of the solution of AscAc was withdrawn with a degassed syringe and injected into the polymerization solution. During polymerization, five aliquots of the solution of AscAc were withdrawn with a degassed syringe and injected into the polymerization solution at regular 1 h-intervals. The monomer conversion and evolution of polymer molar mass were monitored by withdrawing samples during the polymerization and analyzing them with ^{1}H NMR and GPC, respectively. When the desired conversion was reached, the polymerization was stopped by opening the vials to the air. Then, the polymerization solution was mixed with THF and passed through a column filled with neutral alumina to remove the Cu catalyst. The solution was then dialyzed (MWCO 1 kDa) against water for 2 days. The final polymer was freeze-dried to remove water, dried in an oven at 80 °C, and kept in a fridge. The effective removal of solvents and monomer was verified by ^{1}H NMR. The polymerization of (OEG)As followed a similar procedure, except that NaBr was not introduced into the polymerization mixture and AscAc was introduced all at once at the beginning of the polymerization (0.5 equiv relative to Cu).

4.3. Preparation of Polymer Electrolytes

Polymer electrolytes were prepared by mixing the purified polymer P(OEG)$_8$MA, P(OEG)$_p$MA, P(OEG)$_{mp}$MA, P(OEG)$_X$MA, P-(OEG)$_8$A, and P(OEG)$_p$A with LiTFSI. When small amounts of polymers were used, the salt was dissolved in anhydrous THF and the required amount of solution was withdrawn and added to the polymer. The mixture of polymers and salt were dried overnight in an oven at 80 °C. Polymer electrolyte samples were stored in an Ar-filled glovebox (relative humidity <0.1% and O_2 content <20 ppm). The amount of salt was calculated according to the desired r value, expressed as r = [Li$^+$]/[EO]. The following molar masses of the macromonomers and (average) number of EO units were used for the different polymers: (i) P(OEG)$_8$MA: M_n = 452 g mol^{-1}, #EO = 8; (ii) P(OEG)$_p$MA: M_n = 466 g mol^{-1}, #EO = 8.4; (iii) P(OEG)$_{mp}$MA: M_n = 471 g mol^{-1}, #EO = 8.5; (iv) P(OEG)$_X$MA: M_n = 471 g mol^{-1}, #EO = 8.5. As a result, the fraction of salt in each polymer electrolyte was approximately 9.2−9.3, 20.3−20.6, 28.9−29.3, and 33.7−34.1 wt % for r = 0.02, 0.05, 0.08, and 0.1, respectively. For polyacrylates: (i) P(OEG)$_8$MA: M_n = 438 g mol^{-1}, #EO = 8; (ii) P(OEG)$_p$A: M_n = 461 g mol^{-1}, #EO = 8.5. As a result, the fraction of salt in each polymer electrolyte was approximately 9.5−9.6, 20.8−20.9, 29.6−29.8, and 34.4−34.6 wt % for r = 0.02, 0.05, 0.08, and 0.1, respectively.

■ ASSOCIATED CONTENT

Supporting Information

The Supporting Information is available free of charge at https://pubs.acs.org/doi/10.1021/acs.chemmater.5c03475.

Detailed list of employed materials and instruments, characterizations of macromonomers and polymers via HPLC-ESI/MS, ^{1}H NMR, GPC, and TGA, polymerization kinetics, rheology data, and HR and HR-MAS ^{1}H NMR data and spectra (PDF)

■ AUTHOR INFORMATION

Corresponding Authors

Franca Castiglione − *Department of Chemistry, Materials and Chemical Engineering "G. Natta", Politecnico di Milano, 20133 Milano, Italy*; orcid.org/0000-0003-2413-8808; Email: franca.castiglione@polimi.it

Francesca Lorandi − *Laboratory for Macromolecular and Organic Chemistry, Department of Chemical Sciences, University of Padova, 35131 Padova, Italy*; orcid.org/0000-0001-5253-8468; Email: francesca.lorandi@unipd.it

https://doi.org/10.1021/acs.chemmater.5c03475
Chem. Mater. 2026, 38, 2063−2071

Authors

Anna Vigolo − *Laboratory for Macromolecular and Organic Chemistry, Department of Chemical Sciences, University of Padova, 35131 Padova, Italy*

Valeria Vanoli − *Department of Chemistry, Materials and Chemical Engineering "G. Natta", Politecnico di Milano, 20133 Milano, Italy*

Luca Laugeni − *DICMaPI, Università degli Studi di Napoli, 80125 Napoli, Italy*

Carlos Pavón − *Laboratory for Macromolecular and Organic Chemistry, Department of Chemical Sciences, University of Padova, 35131 Padova, Italy;* orcid.org/0009-0001-8619-6643

Rossana Pasquino − *DICMaPI, Università degli Studi di Napoli, 80125 Napoli, Italy*

Edmondo M. Benetti − *Laboratory for Macromolecular and Organic Chemistry, Department of Chemical Sciences, University of Padova, 35131 Padova, Italy;* orcid.org/0000-0002-5657-5714

Complete contact information is available at: https://pubs.acs.org/10.1021/acs.chemmater.5c03475

Notes

The authors declare no competing financial interest.

■ ACKNOWLEDGMENTS

The authors are grateful to Prof. Carla Marega for thermogravimetric analysis. Funding from the Italian Ministry for Universities and Research (MUR) and the European Union-Next Generation EU, Missione 4, Componente 1 through the PRIN PNRR 2022 project UPLiFT (CUP C53D23008380001) is gratefully acknowledged.

■ REFERENCES

(1) Mindemark, J.; Lacey, M. J.; Bowden, T.; Brandell, D. Beyond PEO—Alternative host materials for Li+-conducting solid polymer electrolytes. *Prog. Polym. Sci.* **2018**, *81*, 114−143.

(2) Xue, Z.; He, D.; Xie, X. Poly(ethylene oxide)-based electrolytes for lithium-ion batteries. *J. Mater. Chem. A* **2015**, *3* (38), 19218−19253.

(3) Tan, J.; Guo, L.; Hu, J.; Liu, S. Recent Advances in Poly(ethylene oxide)-Based Solid-State Electrolytes for Lithium-Ion Batteries. *J. Phys. Chem. C* **2024**, *128* (41), 17197−17218.

(4) Gentekos, D. T.; Sifri, R. J.; Fors, B. P. Controlling polymer properties through the shape of the molecular-weight distribution. *Nat. Rev. Mater.* **2019**, *4* (12), 761−774.

(5) Whitfield, R.; Truong, N. P.; Messmer, D.; Parkatzidis, K.; Rolland, M.; Anastasaki, A. Tailoring polymer dispersity and shape of molecular weight distributions: methods and applications. *Chem. Sci.* **2019**, *10* (38), 8724−8734.

(6) Rosenbloom, S. I.; Gentekos, D. T.; Silberstein, M. N.; Fors, B. P. Tailor-made thermoplastic elastomers: customisable materials via modulation of molecular weight distributions. *Chem. Sci.* **2020**, *11* (5), 1361−1367.

(7) Dearman, M.; Ogbonna, N. D.; Amofa, C. A.; Peters, A. J.; Lawrence, J. Versatile strategies to tailor the glass transition temperatures of bottlebrush polymers. *Polym. Chem.* **2022**, *13* (34), 4901−4907.

(8) Lo Bocchiaro, A.; Pavón, C.; Lorandi, F.; Benetti, E. M. Discreteness and dispersity in the design of polymeric materials. *Prog. Polym. Sci.* **2025**, *167*, 101992.

(9) Xu, H.; Greve, E. M.; Mahanthappa, M. K. Morphological Impact of Segment Dispersity in Lithium Salt-Doped Poly(styrene)/Poly(ethylene oxide) Triblock Polymers. *Macromolecules* **2019**, *52* (15), 5722−5734.

(10) Xu, H.; Mahanthappa, M. K. Ionic Conductivities of Broad Dispersity Lithium Salt-Doped Polystyrene/Poly(ethylene oxide) Triblock Polymers. *Macromolecules* **2021**, *54* (18), 8798−8809.

(11) Shioiri, R.; Kokubo, H.; Horii, T.; Kobayashi, Y.; Hashimoto, K.; Ueno, K.; Watanabe, M. Polymer electrolytes based on a homogeneous poly (ethylene glycol) network and their application to polymer actuators. *Electrochim. Acta* **2019**, *298*, 866−873.

(12) Tosa, M.; Hashimoto, K.; Kokubo, H.; Ueno, K.; Watanabe, M. Effect of network homogeneity on mechanical, thermal and electrochemical properties of solid polymer electrolytes prepared by homogeneous 4-arm poly (ethylene glycols). *Soft Matter* **2020**, *16* (17), 4290−4298.

(13) Li, S.; Lorandi, F.; Wang, H.; Liu, T.; Whitacre, J. F.; Matyjaszewski, K. Functional polymers for lithium metal batteries. *Prog. Polym. Sci.* **2021**, *122*, 101453.

(14) Fan, H.; Yang, C.; Wang, X.; Liu, L.; Wu, Z.; Luo, J.; Liu, R. UV-curable PVdF-HFP-based gel electrolytes with semi-interpenetrating polymer network for dendrite-free Lithium metal batteries. *J. Electroanal. Chem.* **2020**, *871*, 114308.

(15) Liu, R.; Wu, Z.; He, P.; Fan, H.; Huang, Z.; Zhang, L.; Chang, X.; Liu, H.; Wang, C.-a.; Li, Y. A self-standing, UV-cured semi-interpenetrating polymer network reinforced composite gel electrolytes for dendrite-suppressing lithium ion batteries. *J. Materiomics* **2019**, *5* (2), 185−194.

(16) Wang, M.; Zhang, H.; Li, Y.; Liu, R.; Yang, H. A three-dimensional co-continuous network structure polymer electrolyte with efficient ion transport channels enabling ultralong-life all solid-state lithium metal batteries. *J. Energy Chem.* **2024**, *94*, 635−645.

(17) Itoh, T.; Fujita, K.; Uno, T.; Kubo, M. Polymer electrolytes based on vinyl ethers with various EO chain length and their polymer electrolytes cross-linked by electron beam irradiation. *Ionics* **2017**, *23*, 257−264.

(18) Geng, Z.; Schauser, N. S.; Lee, J.; Schmeller, R. P.; Barbon, S. M.; Segalman, R. A.; Lynd, N. A.; Hawker, C. J. Role of Side-Chain Architecture in Poly(ethylene oxide)-Based Copolymers. *Macromolecules* **2020**, *53* (12), 4960−4967.

(19) Butzelaar, A. J.; Röring, P.; Mach, T. P.; Hoffmann, M.; Jeschull, F.; Wilhelm, M.; Winter, M.; Brunklaus, G.; Théato, P. Styrene-Based Poly(ethylene oxide) Side-Chain Block Copolymers as Solid Polymer Electrolytes for High-Voltage Lithium-Metal Batteries. *ACS Appl. Mater. Interfaces* **2021**, *13* (33), 39257−39270.

(20) Butzelaar, A. J.; Liu, K. L.; Röring, P.; Brunklaus, G.; Winter, M.; Theato, P. A Systematic Study of Vinyl Ether-Based Poly-(Ethylene Oxide) Side-Chain Polymer Electrolytes. *ACS Appl. Polym. Mater.* **2021**, *3* (3), 1573−1582.

(21) Bennington, P.; Deng, C.; Sharon, D.; Webb, M. A.; de Pablo, J. J.; Nealey, P. F.; Patel, S. N. Role of solvation site segmental dynamics on ion transport in ethylene-oxide based side-chain polymer electrolytes. *J. Mater. Chem. A* **2021**, *9* (15), 9937−9951.

(22) Ji, X.; Xiao, L.-L.; Zhang, Y.; Yue, K.; Zhou, X.; Guo, Z.-H. Unveiling the side-chain effect on ionic conductivity of poly(ethylene oxide)-based polymer-brush electrolytes. *ACS Appl. Energy Mater.* **2022**, *5* (7), 8410−8418.

(23) Barteau, K. P.; Wolffs, M.; Lynd, N. A.; Fredrickson, G. H.; Kramer, E. J.; Hawker, C. J. Allyl Glycidyl Ether-Based Polymer Electrolytes for Room Temperature Lithium Batteries. *Macromolecules* **2013**, *46* (22), 8988−8994.

(24) Wu, Z.; Wang, Y.; Du, W.; Shen, K.; Chen, B.; Pan, H.; Wu, Y.; Lu, Y. Controlled radical polymerization-derived solid-state polymer electrolytes for lithium batteries. *EnergyChem* **2025**, *7* (4), 100160.

(25) Ogbonna, N. D.; Guragain, P.; Mayandi, V.; Sadrinia, C.; Danrad, R.; Jois, S.; Lawrence, J. Discrete Brush Polymers Enhance 19F MRI Performance through Architectural Precision. *J. Am. Chem. Soc.* **2025**, *147* (19), 16171−16178.

(26) Pavón, C.; Ongaro, A.; Filipucci, I.; Ramakrishna, S. N.; Mattarei, A.; Isa, L.; Klok, H.-A.; Lorandi, F.; Benetti, E. M. The Structural Dispersity of Oligoethylene Glycol-Containing Polymer Brushes Determines Their Interfacial Properties. *J. Am. Chem. Soc.* **2024**, *146* (24), 16912−16919.

(27) Pavón, C.; Grigoletto, A.; Kempkes, V.; Eguskiza, A.; Morbidelli, M.; Fiammengo, R.; Papini, E.; Mattarei, A.; Pasut, G.; Matyjaszewski, K.; Lorandi, F.; Benetti, E. M. The Role of Structural Dispersity of Polymer Brushes in Determining the Colloidal Stability of Core−Shell Nanoparticles and Their Interaction with Anti-PEG Antibodies. *JACS Au* **2025**, *5* (9), 4519−4529.
(28) Chen, J.; Rizvi, A.; Patterson, J. P.; Hawker, C. J. Discrete Libraries of Amphiphilic Poly(ethylene glycol) Graft Copolymers: Synthesis, Assembly, and Bioactivity. *J. Am. Chem. Soc.* **2022**, *144* (42), 19466−19474.
(29) Wang, Y.; Tan, X.; Zhang, Y.; Hill, D. J. T.; Zhang, A.; Kong, D.; Hawker, C. J.; Whittaker, A. K.; Zhang, C. Discrete Side Chains for Direct Tuning Properties of Grafted Polymers. *Macromolecules* **2024**, *57* (24), 11753−11762.
(30) Deng, C.; Webb, M. A.; Bennington, P.; Sharon, D.; Nealey, P. F.; Patel, S. N.; de Pablo, J. J. Role of Molecular Architecture on Ion Transport in Ethylene oxide-Based Polymer Electrolytes. *Macromolecules* **2021**, *54* (5), 2266−2276.
(31) Vassiliadou, O.; Chrysostomou, V.; Pispas, S.; Klonos, P. A.; Kyritsis, A. Molecular dynamics and crystallization in polymers based on ethylene glycol methacrylates (EGMAs) with melt memory characteristics: From linear oligomers to comb-like polymers. *Soft Matter* **2021**, *17* (5), 1284−1298.
(32) Papamichail, C.; Techlemtzi, O.; Nikolakakou, G.; Glynos, E. Cation Chemistry and Molecular Weight Effects on the Ion Conductivity in PEO-based Electrolytes. *ACS Macro Lett.* **2025**, *14* (2), 225−230.
(33) Murphy, E. A.; Zhang, C.; Bates, C. M.; Hawker, C. J. Chromatographic Separation: A Versatile Strategy to Prepare Discrete and Well-Defined Polymer Libraries. *Acc. Chem. Res.* **2024**, *57* (8), 1202−1213.
(34) Timachova, K.; Watanabe, H.; Balsara, N. P. Effect of molecular weight and salt concentration on ion transport and the transference number in polymer electrolytes. *Macromolecules* **2015**, *48* (21), 7882−7888.
(35) Zheng, Q.; Pesko, D. M.; Savoie, B. M.; Timachova, K.; Hasan, A. L.; Smith, M. C.; Miller, T. F., III; Coates, G. W.; Balsara, N. P. Optimizing Ion Transport in Polyether-Based Electrolytes for Lithium Batteries. *Macromolecules* **2018**, *51* (8), 2847−2858.
(36) Diddens, D.; Heuer, A.; Borodin, O. Understanding the lithium transport within a rouse-based model for a PEO/LiTFSI polymer electrolyte. *Macromolecules* **2010**, *43* (4), 2028−2036.
(37) Diederichsen, K. M.; Buss, H. G.; McCloskey, B. D. The Compensation Effect in the Vogel−Tammann−Fulcher (VTF) Equation for Polymer-Based Electrolytes. *Macromolecules* **2017**, *50* (10), 3831−3840.
(38) Chintapalli, M.; Le, T. N. P.; Venkatesan, N. R.; Mackay, N. G.; Rojas, A. A.; Thelen, J. L.; Chen, X. C.; Devaux, D.; Balsara, N. P. Structure and Ionic Conductivity of Polystyrene-block-poly(ethylene oxide) Electrolytes in the High Salt Concentration Limit. *Macromolecules* **2016**, *49* (5), 1770−1780.
(39) Harun, F.; Chan, C. H.; Guo, Q. Rheology and microscopic heterogeneity of poly (ethylene oxide) solid polymer electrolytes. *Macromol. Symp.* **2017**, *376* (1), 1700040.
(40) Amanchukwu, C. V.; Gunnarsdottir, A. B.; Choudhury, S.; Newlove, T. L.; Magusin, P. C.; Bao, Z.; Grey, C. P. Understanding Lithium-ion Dynamics in Single-ion and Salt-in-polymer Perfluoropolyethers and Polyethyleneglycol Electrolytes using Solid-state NMR. *Macromolecules* **2023**, *56* (10), 3650−3659.
(41) Bresser, D.; Lyonnard, S.; Iojoiu, C.; Picard, L.; Passerini, S. Decoupling segmental relaxation and ionic conductivity for lithium-ion polymer electrolytes. *Mol. Syst. Des. Eng.* **2019**, *4* (4), 779−792.
(42) Adebahr, J.; Forsyth, M.; Gavelin, P.; Jacobsson, P.; Orädd, G. Ion and solvent dynamics in gel electrolytes based on ethylene oxide grafted acrylate polymers. *J. Phys. Chem. B* **2002**, *106* (47), 12119−12123.
(43) Bamford, J. T.; Jones, S. D.; Schauser, N. S.; Pedretti, B. J.; Gordon, L. W.; Lynd, N. A.; Clément, R. J.; Segalman, R. A. Improved mechanical strength without sacrificing li-ion transport in polymer electrolytes. *ACS Macro Lett.* **2024**, *13* (5), 638−643.
(44) Hosseinioun, A.; Nürnberg, P.; Schönhoff, M.; Diddens, D.; Paillard, E. Improved lithium ion dynamics in crosslinked PMMA gel polymer electrolyte. *RSC Adv.* **2019**, *9* (47), 27574−27582.
(45) Choo, Y.; Halat, D. M.; Villaluenga, I.; Timachova, K.; Balsara, N. P. Diffusion and migration in polymer electrolytes. *Prog. Polym. Sci.* **2020**, *103*, 101220.
(46) Lu, G.; Zhang, Y.; Zhang, J.; Du, X.; Lv, Z.; Du, J.; Zhao, Z.; Tang, Y.; Zhao, J.; Cui, G. Trade-offs between ion-conducting and mechanical properties: The case of polyacrylate electrolytes. *Carbon Energy* **2023**, *5* (2), No. e287.
(47) Fong, K. D.; Self, J.; McCloskey, B. D.; Persson, K. A. Ion Correlations and Their Impact on Transport in Polymer-Based Electrolytes. *Macromolecules* **2021**, *54* (6), 2575−2591.

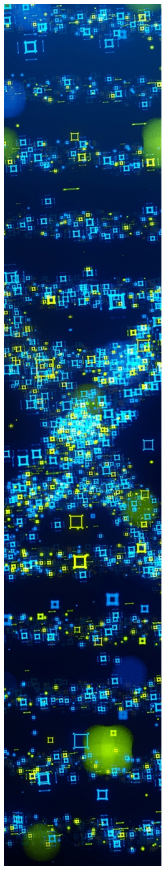
CAS BIOFINDER DISCOVERY PLATFORM™
STOP DIGGING THROUGH DATA —START MAKING DISCOVERIES
CAS BioFinder helps you find the right biological insights in seconds
Start your search
CAS
A division of the American Chemical Society

https://doi.org/10.1021/acs.chemmater.5c03475
Chem. Mater. 2026, 38, 2063−2071